Two-Dimensional NMR Methods for Determining χ_1 Angles of Aromatic Residues in Proteins from Three-Bond $J_{C'C\gamma}$ and $J_{NC\gamma}$ Couplings

Jin-Shan Hu, Stephan Grzesiek, and Ad Bax*

Laboratory of Chemical Physics, National Institute of Diabetes and Digestive and Kidney Diseases, National Institutes of Health, Bethesda, Maryland 20892-0520

Received October 17, 1996

Aromatic residues in proteins typically are very important in the NMR structure determination process because they increase ^{1}H resonance dispersion and they provide large numbers of long-range NOE constraints. The orientation of an aromatic group relative to the polypeptide backbone is defined by the torsion angles χ_1 and χ_2. The χ_2 angle usually equals +90 or −90°, where the sign is of no consequence for Phe and Tyr residues. χ_1 is most commonly found in either −60° or 180° rotameric states.[1] Although, in principle, χ_1 can be obtained from $^3J_{H\alpha H\beta}$ couplings and intraresidue and sequential NOEs,[2] for slowly tumbling proteins, quantitative measurement of these parameters tends to be difficult. Here, we demonstrate that in ^{13}C/^{15}N-enriched proteins the χ_1 angle can readily be determined from two simple quantitative *J* correlation experiments which yield the intraresidue $^3J_{C'C\gamma}$ and $^3J_{NC\gamma}$ coupling constants.

Measurement of $^3J_{CC}$ and $^3J_{NC}$ couplings in proteins has largely been restricted to couplings involving methyl groups[3−6] which, as a result of their favorable relaxation properties and 3-fold degenerate proton resonance, offer exceptional resolution and sensitivity. Here, we exploit the long transverse relaxation times of the backbone ^{15}N and ^{13}C′ to measure ^3J couplings to side-chain C$^\gamma$ resonances of aromatic residues. These ^{13}C$^\gamma$ resonances fall in a relatively narrow region, ranging from ∼110 ppm for Trp to ∼140 ppm for Phe, which permits $^3J_{C'C\gamma}$ and $^3J_{NC\gamma}$ for these residues to be measured using two simple 2D spin-echo difference experiments.

The pulse schemes used for measurement of $^3J_{C'C\gamma}$ and $^3J_{NC\gamma}$ are shown in Figure 1. In the pulse scheme of Figure 1A, H^N magnetization is transferred to its ^{15}N, and after a subsequent semi-constant-time evolution period,[7] it is converted into antiphase C'_yN_z magnetization of the preceding carbonyl. At the midpoint of the subsequent spin-echo delay, 2δ, a selective 180° C′ pulse rephases the effect of $J_{C'N}$, $J_{C'C}$, and $J_{C'H}$ couplings (except for carbonyl−carbonyl/carboxyl couplings, which will attenuate C'_yN_z). If the ^{13}C^{arom} selective 180° pulse is applied at the end of the spin-echo delay (position *a*), the effect of $J_{C'C\gamma}$ couplings in aromatic residues will also refocus. However, when the ^{13}C^{arom} 180° pulse is applied at position *b*, $J_{C'C\gamma}$ dephasing is active for the full period 2δ. Therefore, in this latter case, the C'_yN_z magnetization at the end of the 2δ period,

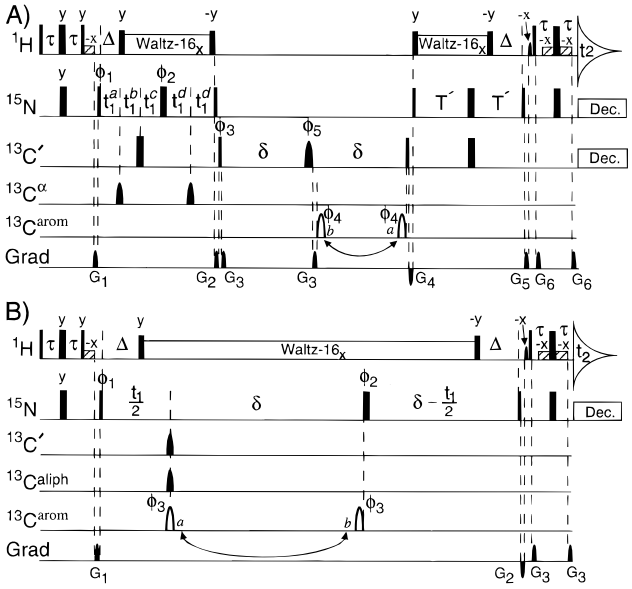

Figure 1. Pulse schemes for (A) the ^{13}C′−{^{13}C$^\gamma$} spin-echo difference and (B) the ^{15}N−{^{13}C$^\gamma$} spin-echo difference ^{1}H−^{15}N HSQC experiments, for measurement of $^3J_{C'C\gamma}$ and $^3J_{NC\gamma}$ in aromatic residues. Narrow and wide rectangular pulses denote 90° and 180° flip angles (except for shaded low-power 90°$_{-x}$ ^{1}H pulses), respectively, and unless indicated the phase is *x*. The shaped low-power ^{1}H 90°$_{-x}$ pulse, the ^{13}C$^\alpha$ 180° pulses, and the 180°$_{\phi 5}$ ^{13}C′ pulse in scheme A have an envelope profile of the center lobe of a sin(*x*)/*x* function and durations of 2 ms, 150 μs, and 260 μs, respectively (for 151 MHz ^{13}C). Open pulses are G3-shaped,[13] and the reference spectrum is recorded using the ^{13}C^{arom} pulse in position *a*, omitting the pulse labeled *b*, whereas the attenuated spectrum is recorded using pulse *b* and omitting pulse *a*. Spectra are recorded in an interleaved manner, i.e., data with the G3 pulse in positions *a* and *b* are recorded and stored separately, before incrementing t_1. RF power: ^{1}H, $\gamma_H B_1 = 27$ kHz (high-power pulses), 220 Hz (low-power pulses), 3.1 kHz (Waltz-16); ^{15}N, $\gamma_N B_2 = 5.3$ kHz (pulses), or 1.0 kHz (Waltz-16). All rectangular ^{13}C′ pulses are applied using RF field strengths of 4.5 kHz at 151 MHz. The duration of the G3 ^{13}C^{arom} 180° pulse is 580 μs, corresponding to an inversion bandwidth of ±18 ppm at 151 MHz ^{13}C. Carrier positions: ^{1}H, H_2O frequency (∼4.65 ppm); ^{13}C′, 176 ppm; ^{13}C^{arom}, 127 ppm; ^{13}C$^\alpha$, 56 ppm; ^{13}C^{aliph}, 43 ppm; ^{15}N, 116.5 ppm. For both schemes, t_1 quadrature is obtained by altering the phase ϕ_1 in the States-TPPI manner. For A, delay durations are as follows: $\tau = 2.25$ ms; $\Delta = 5.4$ ms; $T' = 12.5$ ms; $\delta = 25-50$ ms, depending on the rotational correlation time, τ_c. In order to obtain sufficient resolution in the 2D spectrum, a t_1 acquisition time (AT) longer than $(2J_{NC'})^{-1}$ is needed, and this evolution period is therefore implemented as semi-constant-time[7] rather than constant-time. Thus, for the first t_1 duration, $t_1{}^a(0) = t_1{}^b(0) = t_1{}^d(0) = 7$ ms; $t_1{}^c(0) = 0$; $\Delta t_1{}^a = (\mathrm{AT} - 14\ \mathrm{ms})/2N$, $\Delta t_1{}^b = 7/N$ ms, $\Delta t_1{}^c = (\mathrm{AT} - 28\ \mathrm{ms})/2N$, and $\Delta t_1{}^d = -7/N$ ms, where N is the number of t_1 increments and the spectral width, SW, equals $(\Delta t_1{}^a + \Delta t_1{}^b + \Delta t_1{}^a - 2\Delta t_1{}^d)^{-1} = \mathrm{AT}/N$. Phase cycling: $\phi_1 = x$; $\phi_2 = x, y, -x, -y$; $\phi_3 = 2(x), 2(-x)$; $\phi_4 = 4(x), 4(-x)$; $\phi_5 = 61°$ to compensate for the Bloch−Siegert shift induced by the 180°$_{\phi 4}$ pulse (most easily adjusted by finding the ϕ_5 value which yields zero signal and incrementing that value by 45°); receiver = $x, -x, -x, x$. All gradients are sine-bell shaped, 25 G/cm at their center, with durations $G_{1,2,3,4,5,6} = 3.75$, 1.5, 0.5, 1.65, 1.35, and 0.5 ms. For part B, $\tau = 2.25$ ms, $\Delta = 5.4$ ms, and $\delta = 30-65$ ms, depending on τ_c. All pulse widths and shapes are the same as for scheme A, except for the ^{13}C′ and ^{13}C^{aliph} pulses, which are G3-shaped and have durations of 1.25 ms and 430 μs, respectively. Phase cycling: $\phi_1 = x$; $\phi_2 = x, y, -x, -y$; $\phi_3 = 4(x), 4(-x)$; receiver = $x, -x$. Gradients durations: $G_{1,2,3} = 3.75$, 2.0, and 0.5 ms.

and thereby the intensity in the 2D ^{15}N−^{1}H^N correlation spectrum, is attenuated by $\cos(2\pi J_{C'C\gamma}\delta)$. As δ is known, $J_{C'C\gamma}$ can be calculated from $J_{C'C\gamma} = \cos^{-1}(I_b/I_a)/2\pi\delta$, where I_a and

* Address correspondence to this author at Building 5, Room 126, NIH, Bethesda, MD 20892-0520.

(1) Ponder, J. W.; Richards, F. M. *J. Mol. Biol.* **1987**, *193*, 775−791.
(2) Wagner, G.; Braun, W.; Havel, T. F.; Schaumann, T.; Go, N.; Wüthrich, K. *J. Mol. Biol.* **1987**, *196*, 611−639. Güntert, P.; Braun, W.; Billeter, M.; Wüthrich, K. *J. Am. Chem. Soc.* **1989**, *111*, 3997−4004. Clore, G.. M.; Bax, A.; Gronenborn, A. M. *J. Biomol. NMR* **1991**, *1*, 13−22.
(3) Bax, A.; Max, D.; Zax, D. *J. Am. Chem. Soc.* **1992**, *114*, 6924−6925.
(4) Vuister, G. W.; Wang, A. C.; Bax, A. *J. Am. Chem. Soc.* **1993**, *115*, 5334−5335.
(5) Schwalbe, H.; Rexroth, A.; Eggenberger, T.; Geppert, T.; Griesinger, C. *J. Am. Chem. Soc.* **1993**, *115*, 7878−7879.
(6) Grzesiek, S.; Vuister, G. W.; Bax, A. *J. Biomol. NMR* **1993**, *3*, 487−493.
(7) Grzesiek, S.; Bax, A. *J. Biomol. NMR* **1993**, *3*, 185−204. Logan, T. M.; Olejniczak, E. T.; Xu, R. X.; Fesik, S. W. *J. Biomol. NMR* **1993**, *3*, 225−231.

S0002-7863(96)03625-6 Published 1997 by the American Chemical Society

I_b are the intensities of the $H^N-^{15}N$ correlations in the two experiments with the $^{13}C^{arom}$ 180° pulse applied at positions *a* and *b*, respectively. The C'_yN_z magnetization at the end of the 2δ period of residues other than Phe, Tyr, His, and Trp will be independent of whether the $^{13}C^{arom}$ 180° pulse is applied at time *a* or *b* and will yield identical intensities (except for the random noise contribution) in the two spectra. As magnetization is transferred from the H^N of residue $i+1$ to the $^{13}C'$ of residue *i*, the $J_{C'C\gamma}$ coupling of an aromatic residue *i* is reflected in the intensity ratio of the amide of residue $i+1$. For convenience, the pulse scheme is implemented as a 2D $^1H-^{15}N$ correlation, but it can also be recorded as a $^1H^N-^{13}C'$ spectrum or as a 3D $^1H^N-^{15}N-^{13}C'$ correlation.

The pulse scheme for measurement of $^3J_{NC\gamma}$ (Figure 1B) is analogous to that of Figure 1A, the principal difference being that no transfer to $^{13}C'$ is needed because this experiment measures the $^3J_{NC\gamma}$ dephasing. If T_2 is the transverse relaxation time of ^{15}N in the $^{13}C'/C^\alpha$-coupled mode, it can be shown that, in the limit where $^3J_{NC\gamma} \ll 1/T_2$, optimal sensitivity in the difference spectrum is obtained when $\delta \approx T_2$. Again, $^3J_{NC\gamma}$ is obtained from $J_{NC\gamma} = \cos^{-1}(I_b/I_a)/2\pi\delta$.

In both pulse schemes, water-flip-back procedures[8] are used to avoid saturation of the H_2O signal. This can increase the sensitivity of the experiment, particularly at high pH. For small proteins at low pH, the advantage of the water-flip-back is smaller and the absence of ^1H decoupling during the 2δ period in the scheme of Figure 1A can even decrease the sensitivity of the experiment. Therefore, for the $C'-C^\gamma$ experiments on ubiquitin and calmodulin, ^1H decoupling was not interrupted during the 2δ period, whereas for Nef at pH 8.0, the flip-back procedure as shown in Figure 1A was advantageous.

Experiments were applied to samples of 1.5 mM U-$^{13}C/^{15}N$ ubiquitin, pH 4.3, 30 °C; 1.5 mM of a complex between U-$^{13}C/^{15}N$ calmodulin and a 26-residue unlabeled peptide fragment of skeletal muscle myosin light chain kinase, pH 6.8, 100 mM KCl, 35 °C; and a 0.6 mM sample of HIV-1 U-$^{13}C/^{15}N$ Nef, with deletion of the membrane anchoring 39-residue N-terminal tail and residues 159−173, pH 8.0, 35 °C.

Figure 2A shows the reference spectrum for the calmodulin−peptide complex, obtained with the scheme of Figure 1B and the 180° $^{13}C^{arom}$ pulse in position *a*, together with the $^{15}N-^{13}C^\gamma$ difference spectrum (Figure 2B). Intense correlations for Phe16, Phe65, Phe68, Phe89, His107, Tyr138, and Phe141 correspond to large (~2.5 Hz) $^3J_{NC\gamma}$ couplings, indicative of $\chi_1 = 180°$. Figure 2C shows the analogous difference spectrum for the $^{13}C'-^{13}C^\gamma$ experiment, where the four observed correlations correspond to large (~4.1 Hz) $^3J_{C'C\gamma}$ couplings for Phe12, Phe19, Phe92, and Phe99, indicative of $\chi_1 = -60°$. The difference spectra are free of spurious signals that would have resulted if the selective 180° $^{13}C^{arom}$ pulse had affected either the backbone $^{13}C'$ or $^{13}C^\alpha$ spins. Even for ubiquitin (Supporting Information), for which the signal-to-noise is much higher, no artifacts are observed. Results for calmodulin and ubiquitin agree with their respective X-ray structures,[9,10] but disagree with the rather ill-determined χ_1 angles of Phe16, Phe19, and Phe65 in the original NMR structure of the calmodulin−peptide complex.[11]

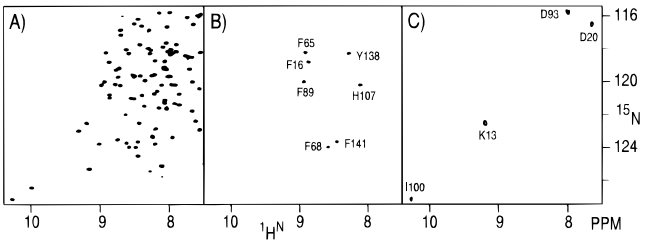

Figure 2. Sections of the 600-MHz $^1H-^{15}N$ correlation spectra of calmodulin complexed with a 26-residue peptide:[11] (A) reference spectrum obtained with the scheme of Figure 1B and the $^{13}C^{arom}$ pulse in position *a*; (B) $^{15}N-\{^{13}C^\gamma\}$ difference spectrum, showing correlations for the calmodulin amide ^{15}N nuclei with a significant coupling (>1.5 Hz) to an aromatic $^{13}C^\gamma$ spin (total recording time, 2.3 h; 2 × 195* × 512* acquired matrix size); (C) $^{13}C'-\{^{13}C^\gamma\}$ difference spectrum, obtained with the scheme of Figure 1A, showing correlations for the calmodulin amide ^{15}N nuclei for which the preceding $^{13}C'$ has a significant coupling (>2 Hz) to an aromatic $^{13}C^\gamma$ spin (total recording time, 7 h; 2 × 70* × 512* matrix size). The dephasing duration, 2δ, was 128 ms for the $^{15}N-\{^{13}C^\gamma\}$ difference spectrum and 100 ms for the $^{13}C'-\{^{13}C^\gamma\}$ difference spectrum.

The experiments are applicable to proteins with less-than-ideal NMR properties. As shown in the Supporting Information, the experiments were also applied to a 0.6 mM sample of HIV-1 Nef, a protein which exhibits relatively large line widths, corresponding to an effective rotational correlation time of *ca.* 12 ns. The resulting spectra yielded χ_1 information for 18 of the 23 assigned aromatic residues. For five of these, the χ_1 angle was undetermined in the set of structures calculated without information from the $^{15}N-^{13}C^\gamma$ and $^{13}C'-^{13}C^\gamma$ difference experiments, despite extensive analysis of NOE, ROE, and *J* couplings other than $^3J_{C'C\gamma}$ and $^3J_{NC\gamma}$.

In summary, we have demonstrated that $^3J_{C'C\gamma}$ and $^3J_{NC\gamma}$ couplings for aromatic residues can readily be measured using simple and sensitive 2D NMR experiments. Except for residues with low backbone order parameters, the $^3J_{C'C\gamma}$ and $^3J_{NC\gamma}$ couplings cluster in relatively narrow ranges: 2.4 ± 0.2 Hz for *trans* $^3J_{NC\gamma}$ and ≤0.5 Hz for *gauche*; 4.0 ± 0.3 Hz for *trans* $^3J_{C'C\gamma}$ and ≤1.1 Hz for *gauche*. This suggests that for aromatic residues χ_1 rotamer averaging is rare. Moreover, the small ranges of the *trans* couplings indicate that the amplitude of χ_1 angle fluctuations for aromatic residues must be quite uniform.[12]

Acknowledgment. We thank F. Delaglio and D. Garrett for data analysis software. This work was supported by the AIDS Targeted Anti-Viral Program of the Office of the Director of the National Institutes of Health. J.-S.H. is supported by a postdoctoral fellowship from the Cancer Research Institute, New York, NY.

Supporting Information Available: Three tables containing the $^3J_{NC\gamma}$ and $^3J_{C'C\gamma}$ values measured for ubiquitin, calmodulin, and Nef and two figures showing the reference and $N-C^\gamma$ and $C'-C^\gamma$ difference spectra for ubiquitin and Nef (5 pages). See any current masthead page for ordering and Internet access instructions.

JA963625Z

(8) Grzesiek, S.; Bax, A. *J. Am. Chem. Soc.* **1993**, *115*, 12593−12594; Kay, L. E.; Xu, G. Y.; Yamazaki, T. *J. Magn. Reson. Ser. A* **1994**, *109*, 129−133.
(9) Meador, W. E.; Means, A. R.; Quiocho, F. A. *Science* **1992**, *257*, 1251−1255.
(10) Vijay-Kumar, S.; Bugg, C. E.; Cook, W. J. *J. Mol. Biol.* **1987**, *194*, 531−544.
(11) Ikura, M.; Clore, G. M.; Gronenborn, A. M.; Zhu, G.; Klee, C. B.; Bax, A. *Science* **1992**, *256*, 632−638.
(12) Brüschweiler, R.; Case, D. A. *J. Am. Chem. Soc.* **1994**, *116*, 11199−11200.
(13) Emsley, L.; Bodenhausen, G. *Chem. Phys. Lett.* **1990**, *165*, 469−476.